

Optimization of LPDA Excitations and the PBM Antenna Benchmarks Using SHADE and L-SHADE Algorithms

Richard A. Formato^{1, *} and Mahamed G. H. Omran²

Abstract—The SHADE and L-SHADE variants of the Differential Evolution global search and optimization algorithm are used to compute optimized excitations for a Log Periodic Dipole Array antenna and to numerically solve the Pantoja-Bretones-Martin suite of antenna benchmark problems. Comparison to published data shows that SHADE and L-SHADE both are effective and efficient algorithms for solving the array excitation problem and the Pantoja-Bretones-Martin wire antenna benchmarks. L-SHADE clearly is more efficient on the array problem, but overall on the benchmarks the opposite is true, albeit to a lesser degree. The data support the view that neither algorithm is generally better than the other for the type of wire antenna problems considered here. Rather, which algorithm is more efficient is highly dependent on the specific antenna being optimized. In terms of the quality of their solutions, however, both algorithms accurately return the benchmarks' known global optima while both converge on different optimal array excitations that result in very similar objective function fitnesses.

1. INTRODUCTION

Global search and optimization algorithms (GSO) have become an important tool in antenna design and optimization (DO). A plethora of algorithms has been applied to a wide range of problems, for example: invasive weed optimization of a PCB UWB antenna [1]; genetic algorithm (GA), particle swarm (PSO) and differential evolution (DE) optimization of circular arrays [2]; GA design of a mobile base station antenna [3]; binary DE antenna design [4]; sparse array design using self-adaptive DE [5]; planar array synthesis using modified PSO [6]; DE/PSO/GA optimization of microstrip antennas [7]; sidelobe and null level optimization with ant colony optimization (ACO) [8]; wideband antenna design using hybrid DE and ACO [9]; and linear array synthesis using DE with convex programming [10]. While these examples emphasize DE because the SHADE algorithms are DE variants, there are many other algorithms applied to antenna DO (see, for example, [11–19]). These are but a few representative examples drawn from hundreds, perhaps thousands, of GSO-based antenna DO problems.

This paper introduces the mix of two new algorithms: SHADE and L-SHADE, both variants of Differential Evolution. They are tested against several antenna optimization problems: (i) determining excitations in a Log Periodic Dipole Array (LPDA) antenna, and (ii) solving the five antenna problems comprising the Pantoja-Bretones-Martin (PBM) benchmark suite [20]. Section 2 of this paper describes SHADE and L-SHADE. Section 3 discusses the LPDA problem and Section 4 the PBM problems. The data show that SHADE and L-SHADE are very effective and efficient optimizers for the type of antenna DO considered here. Section 5 is the Conclusion. The Appendix describes the PBM benchmarks in detail.

Received 7 October 2017, Accepted 17 November 2017, Scheduled 4 December 2017

* Corresponding author: Richard A. Formato (rf2@ieee.org).

¹ Consulting Engineer & Reg. Patent Attorney, Of Counsel Emeritus, Cataldo & Fisher, LLC, P. O. Box 1714, Harwich, MA 02645, USA. ² Department of Computer Science, Gulf University for Science and Technology, Kuwait.

2. SHADE AND L-SHADE ALGORITHMS

Differential Evolution (DE) was proposed by Storn and Price [21] to find the global optimum of nonlinear, non-convex, multimodal, and non-differentiable functions defined in a continuous search space. DE and its variants stand out as very competitive optimizers that have been successfully used to solve many real-world engineering problems [22]. DE is known for its simple structure, ease of use, robustness, and speed [23]. Many attempts have been made to improve DE's performance, two recent and efficient ones being Success-History based parameter Adaptation DE (SHADE) [24] and its improved variant L-SHADE [25]. SHADE ranked third out of twenty one algorithms in the 2013 IEEE CEC competition on real parameter single-objective optimization (the first two ranked algorithms were non-DE) [26]. In the 2014 IEEE CECE competition on real parameter single-objective optimization L-SHADE yielded the best performance among all non-hybrid algorithms [27].

2.1. Canonical Differential Evolution

A DE population is a set of real-parameter vectors $\mathbf{x}_i = \langle x_1, \dots, x_D \rangle$ where $i \in \{1, 2, \dots, N\}$, and D is the problem's dimensionality.

First, a population of potential solutions is randomly generated within the search or decision space (DS) constrained by its lower and upper bounds, \mathbf{a} and \mathbf{b} , respectively, using the following formula:

$$x_{i,j}(0) = a_j + r(b_j - a_j) \quad (1)$$

where r is a uniformly-distributed random number generated from the interval $[0,1]$, $i \in \{1, 2, \dots, N\}$, and $j \in \{1, 2, \dots, D\}$.

After initializing its population, the DE algorithm comprises three steps that are repeated until a stopping criterion is satisfied: (i) Mutation; (ii) Crossover; and (iii) Selection. The DE algorithm is briefly shown as Alg. 1 in Fig. 1, and its three steps are explained below.

Alg. 1: The canonical DE algorithm.

```

initialization
while a stopping criterion is not satisfied do
    for each vector in the population do
        mutation
        crossover
        selection
    endfor
endwhile

```

Figure 1. Differential evolution pseudocode.

2.1.1. Mutation

A *mutant* vector, \mathbf{v}_i , is created for each population member, \mathbf{u}_i , in the current iteration as follows.

$$\mathbf{v}_i(t) = \mathbf{x}_{r_1}(t) + F(\mathbf{x}_{r_2}(t) - \mathbf{x}_{r_3}(t)) \quad (2)$$

where r_1 , r_2 , and r_3 are randomly chosen from $[1, N]$ such that they differ from each other as well as from i . The *scaling factor*, F , is a positive parameter ($F \in (0, 1]$) that controls the magnitude of the difference vector. Eq. (2) describes **DE/rand/1**, which is the most commonly used mutation strategy. Another mutation strategy, **DE/current-to-best/1**, employs the following equation to generate a mutant vector:

$$\mathbf{v}_i(t) = \mathbf{x}_i(t) + F(\mathbf{x}_{best}(t) - \mathbf{x}_i(t)) + F(\mathbf{x}_{r_1}(t) - \mathbf{x}_{r_2}(t)) \quad (3)$$

where $\mathbf{x}_{best}(t)$ is the best individual vector in the population at iteration t (in a minimization problem, for example, it is the vector with the smallest objective function value). If $F < 1$, then the vector being perturbed is the convex combination of $\mathbf{x}_i(t)$ and $\mathbf{x}_{best}(t)$.

2.1.2. Crossover

A trial vector, $\mathbf{u}_i(t)$, is generated by mixing the components of the target vector, $\mathbf{x}_i(t)$, and the mutant vector, $\mathbf{v}_i(t)$, as follows.

$$u_{i,j}(t) = \begin{cases} v_{i,j} & \text{if } j = J \text{ or } r \leq Cr \\ x_{i,j} & \text{otherwise} \end{cases} \quad (4)$$

where Cr is the pre-fixed *crossover rate*; r is a uniformly distributed random number in $[0, 1)$; and J is a randomly chosen number in the set $\{1, 2, \dots, D\}$, thereby insuring that $\mathbf{u}_i(t)$ inherits at least one component from $\mathbf{v}_i(t)$. This process is called **Binomial Crossover** and is the most commonly used DE crossover operator.

2.1.3. Selection

After generating the set of the trial vectors, a *greedy selection* process is used to determine survivors for the next iteration as follows:

$$\mathbf{x}_i(t+1) = \begin{cases} \mathbf{u}_i(t) & \text{if } f(\mathbf{u}_i(t)) \leq f(\mathbf{x}_i(t)) \\ \mathbf{x}_i(t) & \text{otherwise} \end{cases} \quad (5)$$

where $f(\bullet)$ is the objective function to be optimized (minimized or maximized depending on the problem). The equality in “ \leq ” of Eq. (5) helps DE to navigate “flat” fitness landscapes by reducing the possibility of stagnation [22].

2.2. SHADE

The parameters F and Cr have a profound effect on DE’s performance. Tanabe and Fukunaga therefore proposed the SHADE algorithm [24] to take advantage of their success history in exploring DS. SHADE maintains memory archives M_{Cr} and M_F , respectively, which store a total of H values of Cr and F that have performed well in recent previous iterations.

At each iteration, t , there are two control parameters F_i and Cr_i for each vector \mathbf{x}_i . They are initially set to 0.5, and they are updated by randomly choosing an index r_i in $[1, H]$ and applying the following update equations:

$$F_i \sim \text{Cauchy}(M_{F,r_i}, 0.1) \quad (6)$$

$$Cr_i = \begin{cases} 0 & \text{if } M_{Cr,r_i} = \perp \\ \mathcal{N}(M_{Cr,r_i}, 0.1) & \text{otherwise} \end{cases} \quad (7)$$

where $\text{Cauchy}(M_{F,r_i}, 0.1)$ is a Cauchy-distributed random variable with location parameter M_{F,r_i} and scale parameter 0.1; $\mathcal{N}(M_{Cr,r_i}, 0.1)$ is a Gaussian distribution with mean M_{Cr,r_i} , standard deviation 0.1; and \perp is the *terminal value*. If $F_i > 1$, then $F_i = 1$. If $F_i \leq 0$, then Eq. (6) is repeated until a valid value is generated. Once F_i is determined, then Cr_i is updated according to Eq. (7). If the new value of $Cr_i \notin [0, 1]$, then it is replaced by the boundary value, that is 0 or 1, closest to the generated value.

After F_i and Cr_i have been updated for each vector \mathbf{x}_i , a mutant vector, $\mathbf{v}_i(t)$, is generated using the **current-to-pbest/1** mutation strategy [28], which is a variant of the **current-to-best/1** strategy discussed in the previous section. The *greediness* of **current-to-pbest/1** is adjusted using a parameter $p \in (0, 1]$ as follows:

$$\mathbf{v}_i(t) = \mathbf{x}_i(t) + F_i(\mathbf{x}_{pbest}(t) - \mathbf{x}_i(t)) + F_i(\mathbf{x}_{r_1}(t) - \mathbf{x}_{r_2}(t)) \quad (8)$$

where $\mathbf{x}_{pbest}(t)$ is randomly chosen from the top $N \times p$ individuals in iteration t . Parameter p balances exploration and exploitation, with smaller values favoring exploitation while larger ones favor exploration.

SHADE maintains diversity in its population by utilizing an *external archive* that contains parent vectors $\mathbf{x}_i(t)$ that are worse than the trial vectors $\mathbf{u}_i(t)$. In Eq. (8), $\mathbf{x}_{r_2}(t)$ is selected from the union of the population and the archive. This procedure improves diversity by including vectors that have produced worse fitnesses at previous iterations. If the archive size exceeds a predefined limit, then randomly selected vectors are deleted to make space for new ones.

If a boundary-constraint violation occurs, then it is corrected as follows:

$$v_{i,j}(t) = \begin{cases} \frac{(a_j + x_{i,j}(t))}{2} & \text{if } v_{i,j}(t) < a_j \\ \frac{(b_j + x_{i,j}(t))}{2} & \text{if } v_{i,j}(t) > b_j \end{cases} \quad (9)$$

After generating the mutant vector $\mathbf{v}_i(t)$, the binomial crossover of Eq. (4) is used to generate the trial vector $\mathbf{u}_i(t)$. After generating all trial vectors, the greedy selection of Eq. (5) is used to create a new population. Values creating a trial vector $\mathbf{u}_i(t)$ that is better than the target vector $\mathbf{x}_i(t)$ are recoded as S_{Cr} and S_F .

This process is repeated iteration-by-iteration, and at the end of each iteration the historical memory contents are updated using Alg. 2 in Fig. 2. At each iteration, the k th ($1 \leq k \leq H$) entries in the two historical memory archives are also updated. Initially set to $k = 1$, this index is incremented when a new element is inserted into the archive. If $k > H$, k is reset to 1. Note that the memory archives are not updated when all vectors at iteration t fail to generate better trial vectors, that is, $S_{Cr} = S_F = \emptyset$.

Alg. 2. Historical memory update algorithm in SHADE.

```

if  $S_{Cr} \neq \emptyset$  and  $S_F \neq \emptyset$  then
  if  $M_{Cr,k,t} == \perp$  or  $\max(S_{Cr}) == 0$  then
     $M_{Cr,k,t+1} = \perp$ 
  else
     $M_{Cr,k,t+1} = \text{mean}_{WL}(S_{Cr})$ 
  endif
   $M_{F,k,t+1} = \text{mean}_{WL}(S_F)$ 
   $k++$ 
  if  $k > H$  then
     $k = 1$ 
  endif
else
   $M_{Cr,k,t+1} = M_{Cr,k,t}$ 
   $M_{F,k,t+1} = M_{F,k,t}$ 
endif

```

Figure 2. DE pseudocode with history data.

Mean values are computed as follows using a weighted Lehmer mean, denoted $\text{mean}_{WL}(S)$, which has the effect of favoring larger values:

$$\text{mean}_{WL}(S) = \frac{\sum_{k=1}^{|S|} w_k S_k^2}{\sum_{k=1}^{|S|} w_k S_k}, \quad (10)$$

$$\text{where } w_k = \frac{\Delta f_k}{\sum_{l=1}^{|S|} \Delta f_l}, \quad \Delta f_k = |f(\mathbf{u}_k(t)) - f(\mathbf{x}_k(t))|.$$

Note that when M_{Cr} is assigned the terminal value \perp , it will remain fixed at \perp until the end of the SHADE run. This characteristic results in changing only one parameter at a time, which tends to slow convergence (actually a desirable property when SHADE is used to solve multimodal problems).

2.3. L-SHADE

Tanabe and Fukunaga further improved SHADE by linearly reducing its population size during the course of a run [25]. The new algorithm, called L-SHADE, starts with an initial population size of N_{init} vectors that is reduced iteration-by-iteration as follows:

$$N(t+1) = \text{round} \left(\left(\frac{N_{init} - N_{\min}}{\max_nfe} \right) nfe + N_{init} \right) \quad (11)$$

where t is the iteration number, N_{\min} the smallest possible value for the population size, nfe the current number of objective function evaluations, and \max_nfe the maximum number of objective function evaluations. In L-SHADE, $N_{\min} = 4$ because the **current-to-pbest** mutation operator, Eq. (8), requires four vectors. Whenever $N(t+1) < N(t)$, only the best $N(t) - N(t+1)$ vectors survive to the next iteration, and the archive size is readjusted according to the then current population size. Numerical experiments have shown that L-SHADE generally outperforms SHADE [25].

2.4. Experimental Setup

The following setup parameters were used for all optimization runs reported here: For SHADE, N was set to 100, and other parameters were set as suggested in the SHADE code posted online by R. Tanabe[†], viz, $p = 0.11$; $H = D$; archive size = $2N$. For L-SHADE, the values of the control parameters were also the same as those in the online source code[†], viz, $N_{init} = 18D$; $p = 0.11$; $H = 5$; archive size = $1.4N$. Twenty five independent runs were made for each antenna problem, and a run was terminated when either of the following criteria was met: (i) no improvement in best solution for 20 consecutive iterations; or (ii) maximum number of function evaluations \max_nfe was reached.

3. LPDA EXCITATION OPTIMIZATION

The objective of the LPDA problem is to determine a set of excitations that produces an omnidirectional H -plane radiation pattern at a set of predefined frequencies. The Log Periodic Dipole Array antenna, introduced by Isbell in 1960 [29], has gained widespread acceptance as a moderate gain broadband structure [30, 31]. Each dipole in the array bears a fixed geometrical relationship to its neighbors that is determined by a single *scaling parameter* τ as follows:

$$\frac{1}{\tau} = \frac{L_{n+1}}{L_n} = \frac{D_{n+1}}{D_n} = \frac{g_{n+1}}{g_n} = \frac{S_{n+1}}{S_n}$$

where L_n , D_n , g_n , and S_n , respectively, are the n th dipole's overall length, element diameter, feed gap length, and spacing from the $(n-1)$ st dipole [31 @ Ch. 11].

With ultra-wideband applications in mind, for example radio astronomy, communications systems, and radar, Yang published in 2010 a theoretical development of the conditions necessary for obtaining constant radiation characteristics from log-periodic arrays [32]. The planar 5-dipole LPDA described in that paper forms the basis for subsequent work on the excitation problem by Lehmensiek and de Villiers [33, 34]. Only numerical optimization can accurately solve the excitation problem because the analytical approach incorrectly assumes only fundamental current modes on each dipole. Consequently, Brute Force optimization was used in [33] and Population-Based Incremental Learning/Nelder–Mead Simplex in [34].

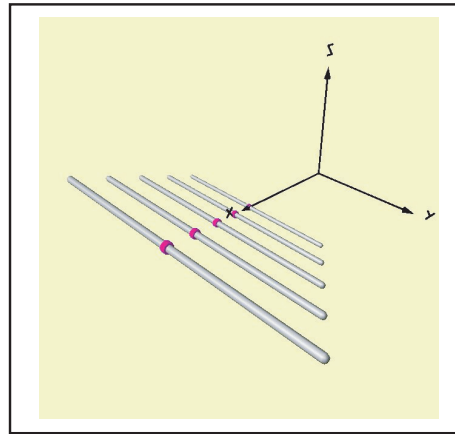
SHADE and L-SHADE are applied to the LPDA problem using the parameters in Section 2.4. The fitness (objective) function, to be minimized, is the deviation from a perfectly uniform (circular) H -plane far field radiation pattern, that is, $\text{Min} [G_{\max}(\theta = 0) - G_{\min}(\theta = 0)]$ where the G 's are maximum and minimum H -plane gains, respectively. The array was modeled with Version 2 of the Numerical Electromagnetics Code [35]. NEC2 is a widely used Method of Moments (MoM) code for modeling wire antennas (in [34] a commercial MoM code was used). For convenience, frequencies and dimensions were scaled to 299.8 MHz ($\lambda = 1$ m). PEC (Perfect Electric Conductor) dipoles are assumed so that conductivity was not scaled.

[†] <https://sites.google.com/site/tanaberyoji/software>.

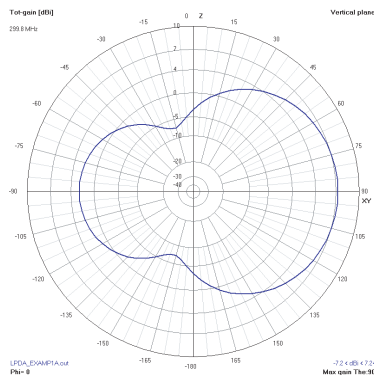
Table 1. 5-Dipole LPDA geometry.

L_n (mm)	R_n (mm)	$X_{0,n}$ (mm)
$68.63\tau^{n-1}$	$0.776\tau^{n-1}$	$40.92\tau^{n-1}$

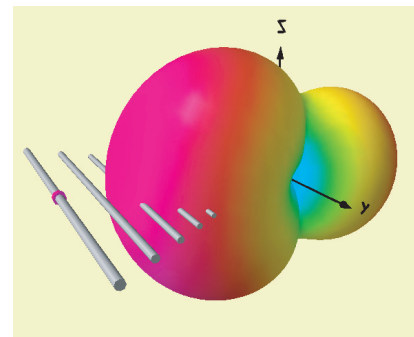
The LPDA geometry is summarized in Table 1 wherein $n = 1, \dots, 5$ and $\tau = \frac{1}{1.18}$ (same value used in [34]). L_n , R_n and $X_{0,n}$, respectively, are the dipole end-to-end length, wire radius, and distance along the $+X$ -axis (NEC employs standard right-handed Cartesian $[x, y, z]$ and spherical $[\rho, \theta, \varphi]$ coordinates). A perspective view of the antenna appears in Fig. 3 (axis length 0.2 m, dipole #1 being the longest). Optimization was performed in the 2.576–4.995 GHz band at the same five logarithmically spaced frequencies used in [34], that is, $f_1 = f_2 \cdot \tau$; $f_2 = 3.04$ GHz; $f_3 = f_2/\tau$; $f_4 = f_2/\tau^2$; and $f_5 = f_2/\tau^3$ (scaled as described above).

**Figure 3.** LPDA perspective view.

The H -plane radiation pattern with only the first dipole excited is shown in Fig. 4. It is highly distorted as expected due to the fields scattered by the other dipoles. When all five dipoles are driven with optimized excitations, however, the resulting pattern is shown in Fig. 5. It is very nearly omnidirectional as required, that is, essentially the pattern of a single dipole without the others being present. Controlling the H -plane pattern is accomplished by using SHADE and L-SHADE to compute an optimized set of excitations that, in effect, render electromagnetically “invisible” all but one of the dipoles.



(a)



(b)

Figure 4. H -plane radiation pattern, only dipole #1 excited.



Figure 5. *H*-plane radiation pattern, 5 dipoles driven, optimized excitation.

Table 2. SHADE optimized 5-frequency LPDA excitations.

Excitation	$f_1 =$ 2.576 GHz	$f_2 =$ 3.040 GHz	$f_3 =$ 3.587 GHz	$f_4 =$ 4.233 GHz	$f_5 =$ 4.995 GHz
V_1	1v $\angle 0^\circ$	1.464v $\angle 301.863^\circ$	1.212v $\angle 286.637^\circ$	0.380v $\angle 316.604^\circ$	1.691v $\angle 41.400^\circ$
V_2	0.852v $\angle 29.698^\circ$	1v $\angle 0^\circ$	1.616v $\angle 345.053^\circ$	2.403v $\angle 330.953^\circ$	2.411v $\angle 91.613^\circ$
V_3	0.607v $\angle 27.823^\circ$	1.775v $\angle 330.345^\circ$	1v $\angle 0^\circ$	2.193v $\angle 295.770^\circ$	2.624v $\angle 58.742^\circ$
V_4	0.815v $\angle 335.746^\circ$	1.773v $\angle 302.798^\circ$	0.701v $\angle 326.215^\circ$	1v $\angle 0^\circ$	1.326v $\angle 31.461^\circ$
V_5	0.281 $\angle 229.808^\circ$	2.545v $\angle 276.356^\circ$	0.066v $\angle 298.975^\circ$	0.559v $\angle 303.709^\circ$	1v $\angle 0^\circ$

Tables 2 and 3, respectively, contain the SHADE- and L-SHADE-computed optimized excitations. Following the protocol used in [34] a reference excitation of 1 volt $\angle 0^\circ$ is applied to the n th dipole at each frequency f_n , $n = 1, \dots, 5$. SHADE returned best fitnesses (maximum deviations from omnidirectional) of 0.02, 0.07, 0.04, 0.01 and 0.03 dB, respectively, at frequencies f_1 , f_2 , f_3 , f_4 , and f_5 . Because NEC2's gain resolution is 0.01 dB, only a value of zero would be better. The corresponding 5-frequency L-SHADE best fitnesses are 0.03, 0.07, 0.07, 0.02 and 0.01 dB. Both SHADE variants achieve quite similar levels of *H*-plane pattern uniformity, neither algorithm being clearly superior to the other, and both returned quite good results from an engineering application point of view. Note that, like [34], this study is limited to determining the required excitations, not implementing them.

Lehmensiek and de Villiers conclude in [34] that there is no unique, well-defined set of excitations that achieves omnidirectionality, their conclusion resting on interpreting the voltage-phase scatter plots in [34]. This hypothesis is supported by the SHADE/L-SHADE data. The optimized excitations in Tables 2 and 3 are quite different, yet they achieve quite similar levels of pattern uniformity, which is convincing evidence that, as suggested in [34], there is no single global optimum. An omnidirectional pattern may be achieved by widely different excitations, and different optimizers will likely return different results that accomplish the same objective.

In addition to the 5-frequency optimization described above, additional eight frequencies were optimized following [34]. Unlike the previous set in which the reference excitation was applied to a different dipole at each frequency, in this case the reference excitation of 1 volt $\angle 0^\circ$ was applied to dipole

Table 3. L-SHADE optimized 5-frequency LPDA excitations.

Excitation	$f_1 =$ 2.576 GHz	$f_2 =$ 3.040 GHz	$f_3 =$ 3.587 GHz	$f_4 =$ 4.233 GHz	$f_5 =$ 4.995 GHz
V_1	1v $\angle 0^\circ$	2.494v $\angle 317.500^\circ$	0.682v $\angle 84.173^\circ$	0.744v $\angle 299.886^\circ$	1.790v $\angle 39.424^\circ$
V_2	0.830v $\angle 352.899^\circ$	1v $\angle 0^\circ$	2.381v $\angle 157.444^\circ$	0.370v $\angle 324.311^\circ$	2.709v $\angle 105.828^\circ$
V_3	0.868v $\angle_{295.789}^\circ$	1.249v $\angle 339.059^\circ$	1v $\angle 0^\circ$	2.181v $\angle 359.349^\circ$	1.847v $\angle 50.911^\circ$
V_4	0.823v $\angle 272.552^\circ$	0.428v $\angle 201.331^\circ$	0.664v $\angle 133.604^\circ$	1v $\angle 0^\circ$	1.734v $\angle 36.704^\circ$
V_5	1.681 $\angle 37.938^\circ$	2.108v $\angle 348.440^\circ$	0.770v $\angle 148.466^\circ$	0.866v $\angle 346.927^\circ$	1v $\angle 0^\circ$

Table 4. SHADE optimized 8-frequency LPDA excitations*.

Frequency (GHz)	V_1	V_2	V_4	V_5
3.14232	1.889v $\angle 310.049^\circ$	1.781v $\angle 353.530^\circ$	0.468v $\angle 321.360^\circ$	0.467v $\angle 381.075^\circ$
3.24808	1.258v $\angle 348.395^\circ$	1.752v $\angle 1.535^\circ$	0.770v $\angle 301.666^\circ$	2.045v $\angle 380.175^\circ$
3.35740	0.816v $\angle 212.072^\circ$	2.484v $\angle 209.305^\circ$	0.093v $\angle 281.402^\circ$	2.903v $\angle 230.544^\circ$
3.47040	1.334v $\angle 37.110^\circ$	2.307v $\angle 73.257^\circ$	1.1018v $\angle 63.801^\circ$	1.700v $\angle 146.014^\circ$
3.7093	0.500v $\angle 310.663^\circ$	0.818v $\angle 327.858^\circ$	0.400v $\angle 398.905^\circ$	0.034v $\angle 152.153^\circ$
3.83273	1.356v $\angle 271.604^\circ$	2.610v $\angle 334.773^\circ$	0.378v $\angle 361.103^\circ$	0.130v $\angle 287.817^\circ$
3.96173	2.128v $\angle 78.369^\circ$	2.742v $\angle 45.671^\circ$	0.059v $\angle 150.336^\circ$	0.269v $\angle 334.196^\circ$
4.09507	1.270v $\angle 288.363^\circ$	2.256v $\angle 306.833^\circ$	2.250v $\angle 6.315^\circ$	1.130v $\angle 324.904^\circ$

* $V_3 = 1v \angle 0^\circ$

#3 at each frequency. Tables 4 and 5, respectively, summarize the SHADE and L-SHADE-computed optimized excitations. As in the previous case, the two algorithms returned quite different optima that nevertheless result in very similar radiation patterns. The SHADE deviations from omnidirectionality are 0.06, 0.06, 0.07, 0.05, 0.06, 0.14, 0.25, 0.14 dB at the eight frequencies ordered lowest to highest. The corresponding L-SHADE values are 0.2, 0.06, 0.05, 0.08, 0.03, 0.17, 0.23, 0.15 dB. Interestingly, both optimizers show an increased deviation at the higher frequencies, but on the whole the deviations are quite similar even though they result from quite different excitations. These data again reinforce the speculation that this antenna problem does not have a unique solution.

Table 5. L-SHADE optimized 8-frequency LPDA excitations*.

Frequency (GHz)	V_1	V_2	V_4	V_5
3.14232	2.255v $\angle 336.261^\circ$	1.934v $\angle 397.182^\circ$	0.204v $\angle 307.550^\circ$	1.337v $\angle 341.448^\circ$
3.24808	1.287v $\angle 308.724^\circ$	2.042v $\angle 309.620^\circ$	0.758v $\angle 300.926^\circ$	1.182v $\angle 357.915^\circ$
3.35740	1.010v $\angle 361.220^\circ$	2.283v $\angle 15.796^\circ$	1.261v $\angle 376.759^\circ$	0.776v $\angle 18.441^\circ$
3.47040	2.004v $\angle 370.422^\circ$	2.680v $\angle 382.074^\circ$	1.340v $\angle 364.680^\circ$	2.352v $\angle 48.624^\circ$
3.7093	1.169v $\angle 312.013^\circ$	2.852v $\angle 348.803^\circ$	1.286v $\angle 387.863^\circ$	0.651v $\angle 325.144^\circ$
3.83273	0.872v $\angle 331.507^\circ$	2.401v $\angle 68.014^\circ$	0.299v $\angle 136.392^\circ$	0.156v $\angle 337.026^\circ$
3.96173	1.199v $\angle 320.160^\circ$	2.259v $\angle 31.574^\circ$	1.639v $\angle 7.927^\circ$	1.476v $\angle 14.482^\circ$
4.09507	1.745v $\angle 298.020^\circ$	2.310v $\angle 341.745^\circ$	2.245v $\angle 364.549^\circ$	1.288v $\angle 327.758^\circ$

* $V_3 = 1v \angle 0^\circ$

Table 6. 5-frequency SHADE statistical data.

Freq. GHz	Fitness				
	Min	Med	Avg	Std Dev	Max
2.576	2.00e-2	9.00e-2	1.07e-1	6.52e-2	2.60e-1
3.040	7.00e-2	2.50e-1	2.42e-1	9.47e-2	4.60e-1
3.587	4.00e-2	2.70e-1	2.59e-1	1.18e-1	4.80e-1
4.233	1.10e-1	2.90e-1	3.05e-1	1.36e-1	5.70e-1
4.995	3.00e-2	1.10e-1	1.09e-1	4.99e-2	2.10e-1

(a)

Freq. GHz	Function Evaluations				
	Min	Med	Avg	Std Dev	Max
2.576	2300	5000	5700	1993	10000
3.040	2300	4400	4576	1808	10000
3.587	2100	4500	5028	2425	10000
4.233	2100	3900	4664	2286	10000
4.995	3800	6000	6380	1999	10000

(b)

Statistical performance data for SHADE and L-SHADE appear in Tables 6 through 9 (*Med* is median, *Avg* arithmetic mean, and *Std Dev* standard deviation). Perhaps the most important statistic is the total number of maximum function evaluations because it measures the algorithms' efficiencies. For the 5-frequency problem the SHADE and L-SHADE figures are 50,000 and 40,902, respectively. For the 8-frequency case the corresponding values are 79,600 and 60,520. L-SHADE thus required about

Table 7. 5-frequency L-SHADE statistical data.

Freq. GHz	Fitness				
	Min	Med	Avg	Std Dev	Max
2.576	3.00e-2	1.00e-1	9.60e-2	5.00e-2	2.00e-1
3.040	7.00e-2	2.10e-1	2.23e-1	1.04e-1	4.80e-1
3.587	7.00e-2	1.90e-1	2.28e-1	1.02e-1	4.00e-1
4.233	2.00e-2	2.60e-1	3.02e-1	1.85e-1	6.70e-1
4.995	1.00e-2	7.00e-2	8.48e-2	6.23e-1	2.50e-1

(a)

Freq. GHz	Function Evaluations				
	Min	Med	Avg	Std Dev	Max
2.576	3159	5132	5236	1211	6955
3.040	2745	4008	4325	1297	8223
3.587	2745	4435	4700	1407	8194
4.233	2745	4985	5167	1517	8616
4.995	3357	6054	6258	1741	8914

(b)

Table 8. 8-frequency SHADE statistical data.

Freq. GHz	Best Fitness				
	Min	Med	Avg	Std Dev	Max
3.14232	6.00e-2	1.80e-1	1.65e-1	7.26e-2	2.90e-1
3.24808	6.00e-2	2.50e-1	2.61e-1	1.26e-1	5.30e-1
3.35740	7.00e-2	2.30e01	2.51e-1	1.20e-1	6.40e-1
3.47040	5.00e-2	2.20e-1	2.27e-1	9.09e-2	4.10e-1
3.7093	6.00e-2	3.40e-1	3.73e-1	1.87e-1	7.70e-1
3.83273	1.40e-1	4.70e-1	5.17e-1	2.31e-1	1.09e0
3.96173	2.50e-1	5.00e-1	5.23e-1	1.83e-1	9.60e-1
4.09507	1.40e-1	4.00e-1	3.97e-1	1.62e-1	8.00e-1

(a)

Freq. GHz	Function Evaluations				
	Min	Me	Avg	Std Dev	Max
3.14232	2400	3900	4516	1867	9800
3.24808	2300	4300	5072	2132	10000
3.35740	2700	4000	4328	1709	10000
3.47040	2500	4500	5084	1885	10000
3.7093	2500	4400	5040	2096	9800
3.83273	2100	4700	5448	2311	10000
3.96173	2200	4400	4904	1929	10000
4.09507	2800	4200	4968	2132	10000

(b)

Table 9. 8-frequency L-SHADE statistical data.

Freq. GHz	Best Fitness				
	Min	Med	Avg	Std Dev	Max
3.14232	2.00e-1	1.20e-1	1.19e-1	4.88e-2	2.10e-1
3.24808	6.00e-2	2.60e-1	2.82e-1	1.52e-1	6.90e-1
3.35740	5.00e-2	2.30e-1	2.38e-1	1.23e-1	5.00e-1
3.47040	8.00e-2	2.20e-1	2.31e-1	1.12e-1	5.30e-1
3.7093	3.00e-2	3.30e-1	3.32e-1	1.58e-1	7.00e-1
3.83273	1.70e-1	4.20e-1	4.54e-1	1.74e-1	8.80e-1
3.96173	2.30e-1	4.90e-1	5.36e-1	2.35e-1	1.07e0
4.09507	1.50e-1	4.20e-1	4.23e-1	1.89e-1	9.30e-1

(a)

Freq. GHz	Function Evaluations				
	Min	Med	Avg	Std Dev	Max
3.14232	3058	5059	5373	1590	8568
3.24808	2638	4517	4578	1078	6811
3.35740	2851	4598	4586	1257	7352
3.47040	3058	4517	4888	1254	7911
3.7093	2745	5059	5011	1526	8729
3.83273	2851	4268	4801	1375	7225
3.96173	2638	4517	4635	1231	7473
4.09507	2638	3737	4131	1084	6451

(b)

18% fewer evaluations for the 5-frequency case and about 24% fewer for the 8-frequency case on the LPDA problem. L-SHADE clearly is superior to SHADE in terms of efficiency while both algorithms are similarly accurate in terms of locating optima.

4. PBM ANTENNA BENCHMARKS

The PBM benchmarks were developed to serve as a standard set of “real world” antenna problems that measure the effectiveness of an antenna optimization algorithm. They are described in detail in the Appendix. The fitness function for each problem is the antenna’s directivity which is to be maximized, that is $\text{Max}[D(x_i)]$, where the x_i are decision variables specific to each problem (see Appendix for details) and where $i = 1, 2$ for problems #1–4 and $i = 1, \dots, N_{el} - 1$ for problem #5, N_{el} being the number of elements in a collinear array. The PBM problems do not have analytical solutions and consequently must be solved numerically. Although there are published results based on analytical solutions [36], those results are incorrect because they make several invalid assumptions, namely (i) sinusoidal current distributions, (ii) filamentary currents, and (iii) no mutual coupling between antenna elements. These assumptions are incorrect for the actual PBM antenna structures and consequently lead to incorrect results. The PBM problems can only be solved numerically.

While any numerical “modeling engine” can be used, the original PBM suite was optimized using NEC Version 2 [35], a widely available freeware version of the program developed at the Lawrence Livermore National Laboratory (US Dept. Energy). Being an MoM code, NEC is intended primarily for modeling wire structures such as the PBM benchmarks.

The PBM suite has been used to assess the performance of several optimization algorithms besides those in the original PBM paper. They include CFO, π CFO, and π GASR.

This paper adds SHADE and L-SHADE to the list and compares their results directly with published data. Because the modeling engine is a separate program, the optimization algorithm calls an independent NEC module that computes the fitness using decision variable values supplied by the optimizer. NEC Ver. 2 was used in the original PBM paper and here for SHADE/L-SHADE; NEC Ver. 4 was used with the other optimizers (both return the same results).

4.1. PBM Best Fitness (Maximum Directivity)

Table 10 tabulates the best fitness returned by each of the tested algorithms. Many of the PBM data are estimated from figures in the original paper and consequently carry a measure of uncertainty. The PBM data also may differ from the other optimizers' because of subtle effects such as compiler or modeling differences, for example, source modeling in NEC. What is important is consistency in the data, and even a cursory glance at Table 10 shows the data are very consistent one algorithm to the next. With respect to how well these algorithms computed the best fitness (antenna maximum directivity), the data show that no algorithm is clearly superior. Each one returned a best fitness value that was at or close to the known maximum. The six algorithms are not distinguishable on that basis.

Table 10. Best fitness.

PBM Benchmark	Maximum Directivity					
	PBM	CFO	π CFO	π GASR	SHADE	L-SHADE
1	3.32	3.20627	3.24340	3.25837	3.20627	3.20627
2a (no noise)	18.3 ⁽¹⁾	18.3654	18.2810	17.9473	18.3654	18.3654
2b (noisy)	<i>nr</i>	18.6880	19.7609	18.8314	19.9670	19.3834
3	7.05⁽¹⁾	6.48634	6.57766	6.57658	6.48634	6.48634
4	5.8 ⁽¹⁾	5.71479	5.29663	5.29663	5.94292	5.94292
5 (6 el)	\sim 11.25	11.2202	11.2202	11.2202	11.2202	11.2202
5 (7 el)	<i>nr</i>	13.1826	13.0918	13.1826	13.1826	13.1826
5 (10 el)	\sim 19	19.0985	19.0985	19.0985	19.0985	19.0985
5 (13 el)	<i>nr</i>	25.0611	25.0035	25.0035	25.0035	25.0035
5 (16 el)	\sim 31	30.9742	30.9742	30.9742	30.9713	30.9742
5 (24 el)	\sim 47	46.8813	46.8813	46.8813	46.7951	46.8813

Notes: ⁽¹⁾ values estimated from the figures in [20]; *nr* — not reported in [20]
values marked \sim are estimated from Fig. 13 in [20].

On PBM problem #1 SHADE and L-SHADE return the same directivity as CFO, which is a value slightly less than π CFO's and π GASR's. π GASR returned the best fitness of 3.25837. On PBM #2(a) just the opposite occurred with CFO, SHADE and L-SHADE all returning a best directivity of 18.3654 while the other algorithms returned slightly lower values. Problem #2(b) is a noisy version of 2(a), details in the Appendix, whose purpose is to investigate how well the location of maximum fitness is determined, not its value because it is inherently random. This metric is discussed in connection with Table 11 which tabulates the best fitness coordinates.

On problem #3 the PBM maximum directivity of 7.05 appears suspicious because all the other optimizers returned values that are substantially lower but consistent with each other. The best value of 6.57766 is returned by π CFO with π GASR's being very slightly less. SHADE, L-SHADE and CFO returned the same value of 6.48634. On PBM #4, SHADE and L-SHADE returned the same best fitness of 5.94292, which is better than the PBM value, and substantially higher than π CFO's and π GASR's, both of which are the same.

Inspection of the data for PBM problem #5 shows a remarkable degree of consistency across all six algorithms. When the best fitnesses differ at all the difference is extremely small, especially on a

Table 11. Best fitness coordinates.

PBM No.	PBM		CFO		π CFO	
	x_1	x_2	x_1	x_2	x_1	x_2
1	2.58λ	0.63	2.5509λ	0.6181	2.5896λ	0.6195
2a (no noise)	$\sim 5.85\lambda$	1.5730	5.9236λ	1.5569	5.9246λ	1.5554
2b (noisy)	$nr^{(1)}$	nr	6.9360λ	1.5472	5.8877λ	1.5560
3	0.5	1.5730	0.4802	1.5733	2.4806	1.5611
4	1.5λ	0.834	1.4952λ	0.7110	1.4913λ	0.7176
Min/Max/ Δ , $d_i, i = 1, \dots, N_{el} - 1$						
5	0.99 λ		0.983/1 λ /0.017		0.974/1.199 λ /0.225	

Notes: ⁽¹⁾ nr — not reported in [20].

(a)

PBM No.	π GASR		SHADE		L-SHADE	
	x_1	x_2	x_1	x_2	x_1	x_2
1	2.5845λ	0.6198	2.5572λ	0.6159	2.5654λ	0.6162
2a (no noise)	6.9270λ	1.5467	5.9178λ	1.5677	5.9222λ	1.5544
2b (noisy)	9.8907λ	1.5230	5.9275λ	1.4975	5.9272λ	1.5807
3	1.5201	1.5704	1.4789	1.5752	1.5205	1.5534
4	1.4942λ	0.7317	1.4999λ	0.7040	1.4993λ	0.7149
Min/Max/ Δ , $d_i, i = 1, \dots, N_{el} - 1$						
5	0.987/1 λ /0.013		0.955/1.022/0.067		0.956/1.029/0.073	

Notes: ⁽¹⁾ nr — not reported in [20].

(b)

fractional basis. A fair reading of these data is that all six algorithms returned essentially the same maximum directivity for the variable-length collinear dipole array.

4.2. PBM Coordinates of Maximum Directivity

Locations in the decision space for the returned best fitnesses are tabulated in Table 11. Because the first four problems are two-dimensional (2D), the table lists the coordinates (x_1, x_2) of the computed maximum. PBM #5, however, is $(N_{el} - 1)D$ where N_{el} is the number of dipole elements in the collinear array. In this case, the table lists the range of coordinate values (minimum/maximum/difference) for the computed best fitness.

On PBM #1, all algorithms returned very similar coordinates, while the PBM values are slightly different. The plots in the Appendix show a broad maximum which readily accounts for slight differences in where the optimizers placed it. For problem #2(a), the maxima locations are all quite similar except for π GASR whose x_1 coordinate is significantly different than the others. This difference explains why π GASR's fitness in Table 10 is significantly less than the known maximum.

PBM #2(b) was included in order to investigate how well an algorithm would locate the maximum directivity's coordinates in the presence of noise. Interestingly, their values were not reported in [20]. Each algorithm returned a similar x_2 value, but their x_1 values exhibit much more variability. This effect is particularly evident in the π GASR coordinate of 9.8907λ compared to the next largest value 6.9360λ returned by CFO.

Problem #3 is interesting because its landscape is very spiky with four global maxima. All six algorithms converged on essentially the same x_2 coordinate in the range 1.5534–1.5752. With respect to x_1 , however, CFO and π CFO located their maxima at different x_1 points, 0.4802 and 2.4806 rad, respectively, while π GASR, SHADE and L-SHADE all converged to $x_1 = \pi/2$. Nevertheless the returned

maxima were quite similar as seen in Table 10.

On PBM #4, each algorithm performed well locating the maximum's coordinates. The results are quite consistent with respect to x_1 (known value 1.5λ). The values also are very consistent with respect to x_2 (0.7040–0.7317), but they do differ from the PBM value of 0.834.

The known coordinate for problem #5's maximum directivity is a uniform separation of 0.99λ between collinear elements regardless of their number. Because each optimizer returns a set of separations that are not all equal, Table 11 lists the minimum and maximum values and their difference. The smaller their difference the closer the algorithm came to locating the known maximum. The tightest cluster was returned by π GASR, the loosest by π CFO. The other three optimizers returned similarly spread element separations. It is significant that in spite of the range of element separations the computed maximum array directivities in Table 10 are remarkably consistent. These data show that the collinear array's directivity is not particularly sensitive to element separation; in other words, its maximum in the $(N_{el} - 1)D$ decision space is fairly broad.

Table 12. SHADE PBM statistical data.

PBM No.	Best Fitness				
	Max	Med	Avg	Std Dev	Min
1	3.2062	3.2062	3.2036	9.21e-3	3.1696
2a (no noise)	18.3654	18.3654	18.3654	3.63e-15	18.3654
2b (noisy)	19.9670	19.3379	19.3950	2.57e-1	18.9463
3	6.4863	6.4863	6.4852	5.96e-3	6.4565
4	5.9429	5.9429	5.9429	9.06e-16	5.9429
5 (6 el)	11.2202	11.2202	11.2202	7.25e-15	11.2202
5 (7 el)	13.1826	13.1826	13.1926	3.63e-15	13.1826
5 (10 el)	19.0985	19.0985	19.0985	1.09e-14	19.0985
5 (13 el)	25.0034	25.0034	25.0034	3.63e-15	25.0034
5 (16 el)	30.9742	30.9742	30.9713	1.42e-2	30.9030
5 (24 el)	46.8813	46.7735	46.7951	4.40e-2	46.7735

(a)

PBM No.	Function Evaluations				
	Min	Med	Avg	Std Dev	Max
1	700	1025	992	174.7	1400
2a (no noise)	800	1075	1112	166.3	1450
2b (noisy)	800	1450	1547	454.9	2700
3	725	1175	1172	252.5	1800
4	725	875	864	58.2	975
5 (6 el)	750	975	964	110.9	1150
5 (7 el)	950	1125	1124	97.8	1300
5 (10 el)	4700	5000	4984	624.5	5000
5 (13 el)	5100	5800	5764	334.0	6400
5 (16 el)	5500	7200	7028	521.6	7800
5 (24 el)	6300	7300	7512	744.6	9400

(b)

Table 13. L-SHADE PBM statistical data.

PBM No.	Best Fitness				
	Max	Med	Avg	Std Dev	Min
1	3.2063	3.2063	3.2033	9.24e-3	3.1670
2a (no noise)	18.3654	18.3654	18.3654	3.63e-15	18.3654
2b (noisy)	19.9764	19.3284	19.3835	2.52e-1	18.9400
3	6.4864	6.4864	6.4846	8.93e-3	6.4417
4	5.9429	5.9429	5.9429	9.06e-16	5.9429
5 (6 el)	11.2202	11.2202	11.2202	7.25e-15	11.2202
5 (7 el)	13.1826	13.1826	13.1826	3.63e-15	13.1826
5 (10 el)	19.0985	19.0985	19.0985	1.09e-14	19.0985
5 (13 el)	25.0035	25.0035	25.0035	3.63e-15	25.0035
5 (16 el)	30.9742	30.9742	30.9742	1.09e-14	30.9742
5 (24 el)	46.8813	46.8813	46.8555	4.70e-2	46.7735

(a)

PBM No.	Function Evaluations				
	Min	Med	Avg	Std Dev	Max
1	723	1051	1031	139.3	1262
2a (no noise)	848	1081	1157	148.1	1421
2b (noisy)	865	1465	1473	329.1	2104
3	865	1302	1309	232.9	1773
4	772	1045	1021	101.2	1190
5 (6 el)	2122	2382	2385	139.3	2573
5 (7 el)	2487	2858	2868	143.4	3093
5 (10 el)	3663	4065	4046	126.6	4222
5 (13 el)	6471	6777	6822	174.6	7188
5 (16 el)	7908	8083	8110	133.8	8439
5 (24 el)	8955	9488	9446	187.8	9679

(b)

4.3. PBM Statistics

Statistical data for the SHADE/L-SHADE PBM runs appear in Tables 12 and 13. As with the LPDA data, perhaps the most important metric is the total number of maximum required function evaluations (FEs). Across all PBM problems that figure for SHADE is 39,375 and for L-SHADE 42,944. This result is quite different than for the LPDA problem. While in that case L-SHADE clearly was the more efficient optimizer, in this case the roles are reversed, but the difference is much smaller with L-SHADE requiring about 9% more FEs. On a problem-by-problem basis, however, the results are more mixed. For example, on PBM #5 7-element SHADE required 1,300 FEs compared to L-SHADE’s 3,093, while for the 10-element case the corresponding values are flipped at 5,000 and 4,222. These data support the conclusions that neither algorithm is clearly superior to the other in terms of computational efficiency and that which one is better is highly dependent on the problem at hand.

5. CONCLUSION

The SHADE and L-SHADE optimization algorithms were applied to several wire antenna problems with quite good results, specifically (i) optimal excitation of a five-element Log Periodic Dipole Array to create an omnidirectional far-field H -plane radiation pattern and (ii) optimization of the five PBM antenna benchmark problems. The algorithms' performance was comparable to or better than that of other algorithms applied to the same problems. While both of these DE variants were comparably accurate in locating global extrema, L-SHADE was more efficient on the LPDA problem (fewer FEs), but not so on the PBM problems. The data suggest that neither algorithm is clearly more efficient for the types of wire antenna problems considered here, and which algorithm is better for a specific problem is highly dependent on the problem itself. As to the LPDA excitation problem, this work does confirm that (i) indeed it is possible to determine a set of excitations that render electromagnetically “invisible” all but one of the dipoles and (ii) that the solution is not unique. With respect to the PBM benchmarks, this work provides results that are consistent with the known solutions and comparable to other optimizers in accuracy and efficiency.

APPENDIX A. PBM BENCHMARKS

A.1 Benchmark #1: Variable Length Center-Fed Dipole

Figure A1 shows the antenna geometry for PBM problem #1. The objective function, as with all the PBM problems, is the center-fed dipole's directivity, D , which is to be maximized as a function of its total length, L , and the polar angle, θ . A perspective view of the 2D landscape is in Fig. A2 with additional plots projecting onto the principal planes in Fig. A3. The topology or “landscape” is $L = \Omega \cup F(X)$ where $\Omega := \{X | x_k^{\min} \leq x_k \leq x_k^{\max}, k = 1, \dots, N_d\}$ is the N_d -dimensional decision space, and $F(X) : X \in \Omega \subset R^n$ is the fitness function being optimized. In this case it is smoothly varying with one global maximum and two similar amplitude local maxima.

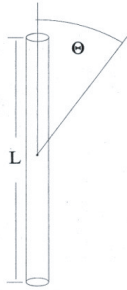


Figure A1. CF dipole.

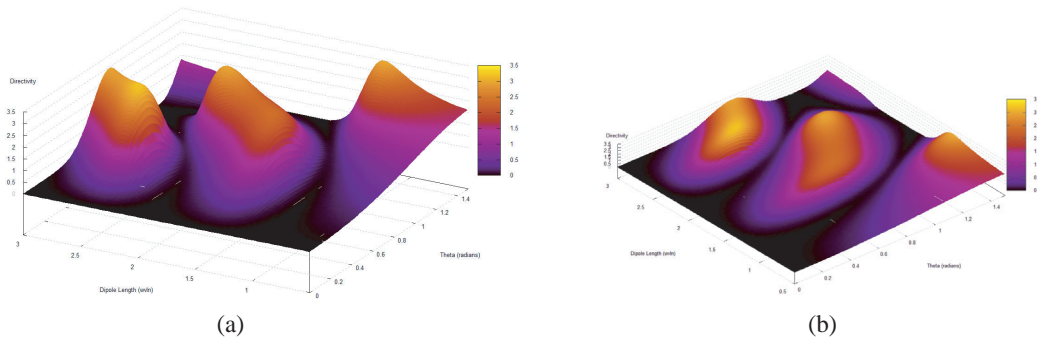


Figure A2. (a) PBM #1 topology, perspective view. (b) PBM #1 perspective view.

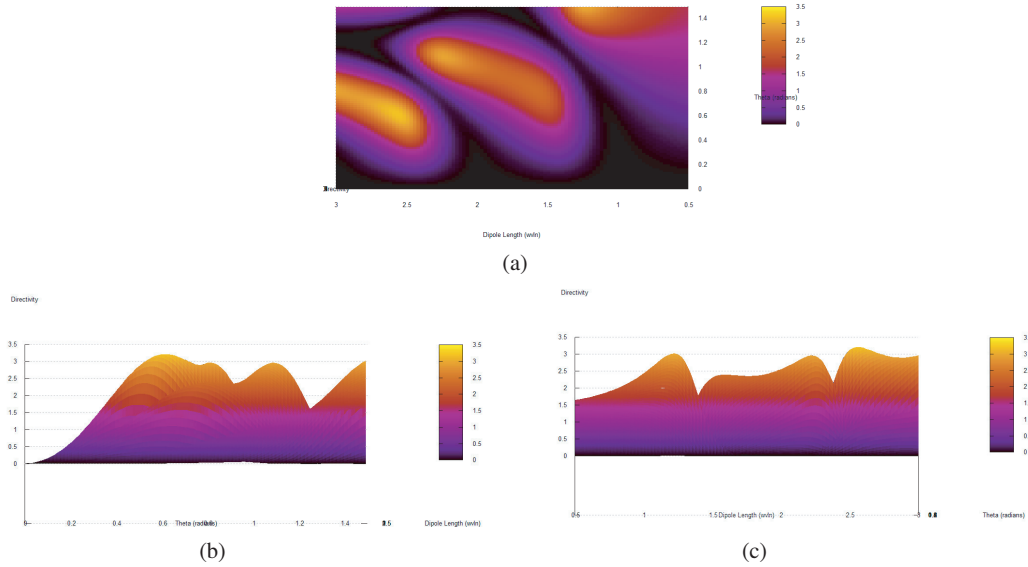


Figure A3. (a) PBM #1 projected onto $L-\theta$ plane. (b) PBM #1 projected onto $\theta-D$ plane. (c) PBM #1 projected onto $L-D$ plane.

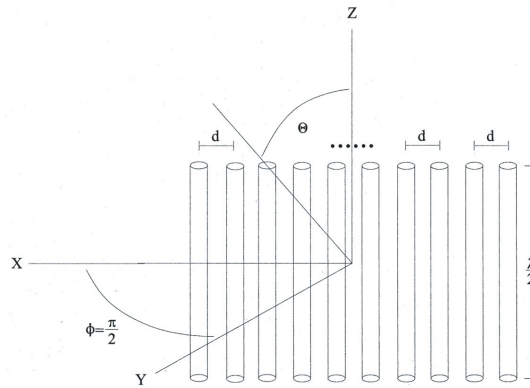


Figure A4. PBM #2, $\lambda/2$ -wave CF in-phase dipoles.

A.2 Benchmark #2: Array of Uniform Half-Wave Dipoles

PBM problem #2 is an array of uniformly spaced $\lambda/2$ dipoles (Fig. A4). All are center-fed with equal amplitude in-phase sources. Also shown is NEC’s right-handed Cartesian coordinate system polar and azimuth angles θ and ϕ , respectively. The objective is maximization of the directivity $D(d, \theta)$ in the plane $\phi = 90^\circ$ as a function of separation d and polar angle θ with and without additive Gaussian noise. Fig. A5 shows the landscape with/without noise. Figs. A6 and A7 show principal plane plots with/without noise. Gaussian noise is generated by adding to NEC’s computed directivity a normally distributed zero-mean, 0.2-variance random variable (rv) z computed using the Box Muller method: $z = \mu + \sigma\sqrt{-2\ln(s)} \cos(2\pi t)$, where μ and σ , respectively, are the mean (0) and standard deviation (0.4472). s and t are rv’s uniformly distributed on $[0, 1]$ generated using the compiler’s internal random number generator seeded with the optimization run’s start time (seconds after midnight to the nearest 0.01 sec).

A.3 Benchmark #3: Circular Array of Half-Wave Dipoles

PBM #3 is a 1λ radius circular array of eight center-fed $\lambda/2$ dipoles deployed parallel to the z -axis uniformly spaced around its circumference (Fig. A8). All are fed with equal-amplitude sources,

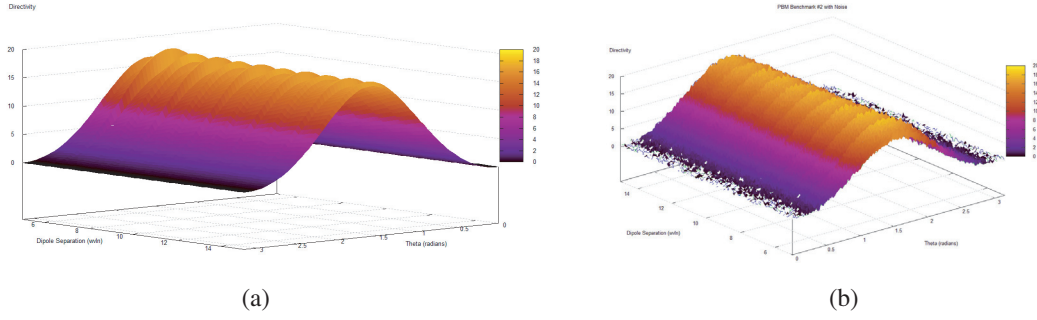


Figure A5. (a) PBM #2 perspective view (no noise). (b) PBM #2, additive Gaussian noise.

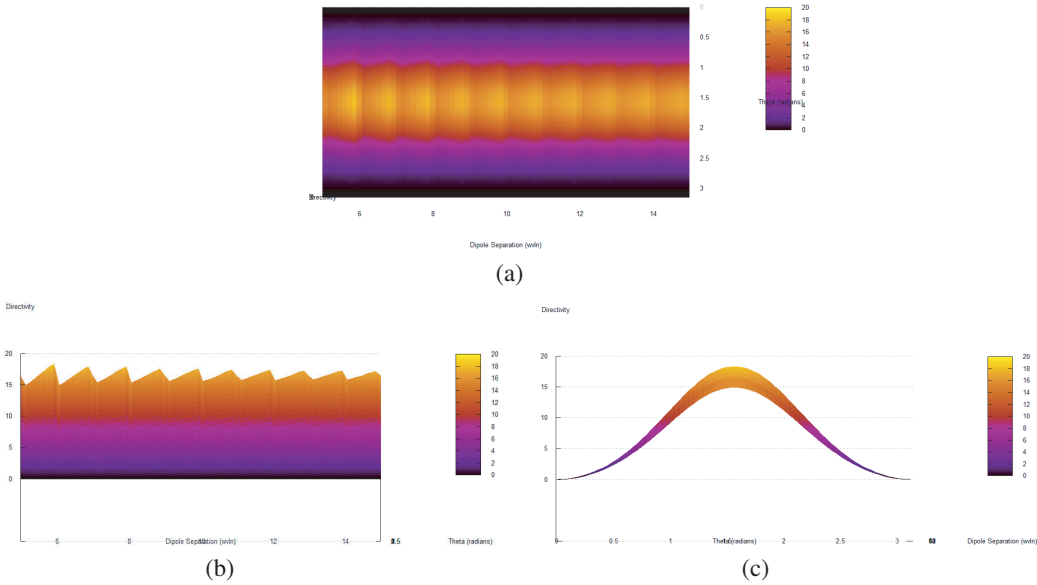


Figure A6. (a) PBM #2, no noise projected onto d - θ plane. (b) PBM #2, no noise, d - D plane. (c) PBM #2, no noise, θ - D plane.

but the phase varies as $\alpha_n = -\cos[2\pi\beta(n-1)]$, $n = 1, \dots, 8$. The unit-amplitude excitation is $V_n = \cos \alpha_n + j \sin \alpha_n$. Directivity $D(\beta, \theta)$ in the plane $\phi = 0^\circ$ is to be maximized as a function of the dimensionless parameter $0 \leq \beta \leq 4$ and the polar angle θ . There are four global maxima at $\beta_i = i - 0.5$, $i = 1, \dots, 4$; $\theta = \frac{\pi}{2}$ (Fig. A9). Principal plane plots are shown in Fig. A10.

A.4 Benchmark #4: Vee Dipole

PBM #4 is the Vee-dipole shown in Fig. A11 comprising two equal-length arms with length L_{arm} subtending inner angle 2α connected by a feed segment of length $2L_{feed}$ excited at its midpoint. Directivity $D(L_{total}, \alpha)$ is to be maximized along the $+X$ -axis as a function of the total length $0.5\lambda \leq L_{total} = 2L_{arm} + 2L_{feed} \leq 1.5\lambda$ and angle $\frac{\pi}{18} \leq \alpha \leq \frac{\pi}{2}$ ($L_{feed} = 0.01\lambda$). Perspective views of the landscape appear in Fig. A12 with principal plane projections in Fig. A13. The Vee's objective function is unimodal with a single global maximum at $D(L_{total}, \alpha) = (1.5\lambda, 0.834)$ in a smoothly varying topology without pronounced local maxima.

A.5 Benchmark #5: N-Element Array of Collinear Dipoles

PBM #5 is the N_{el} -element array of collinear center-fed $\lambda/2$ dipoles in Fig. A14. All elements are excited in-phase with equal amplitude. The objective is maximum directivity at $\phi = 0^\circ$ as a function of the center-to-center spacings $0.5\lambda \leq d_i \leq 1.5\lambda$. Unlike the previous 2D problems, the dimensionality

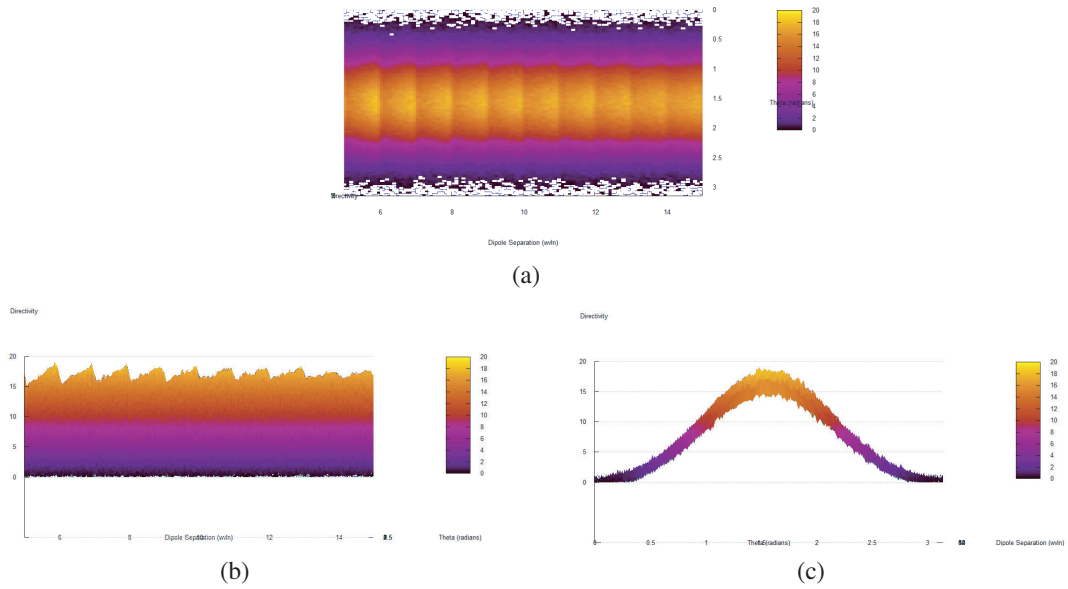


Figure A7. (a) PBM #2 with noise, $d-\theta$ plane. (b) PBM #2 with noise, $d-D$ plane. (c) PBM #2 with noise projected onto $\theta-D$ plane.

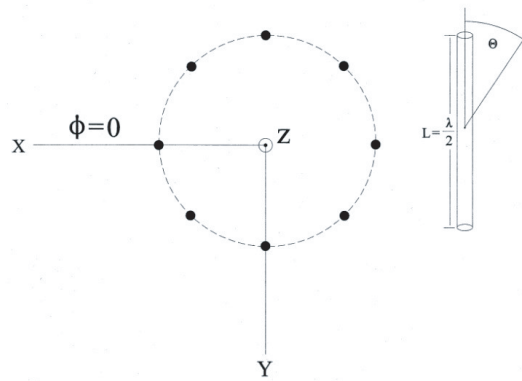


Figure A8. PBM #3 circular array $\lambda/2$ dipoles (1λ radius).

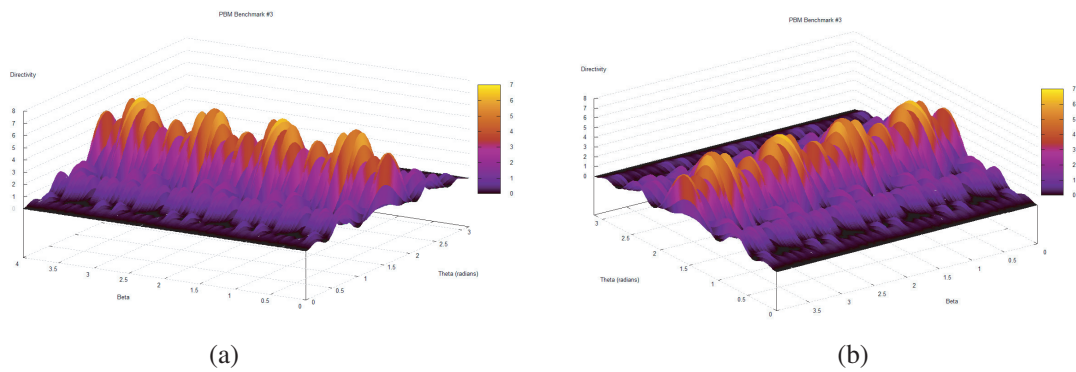


Figure A9. (a) PBM #3 landscape, perspective view. (b) PBM #3 perspective view.

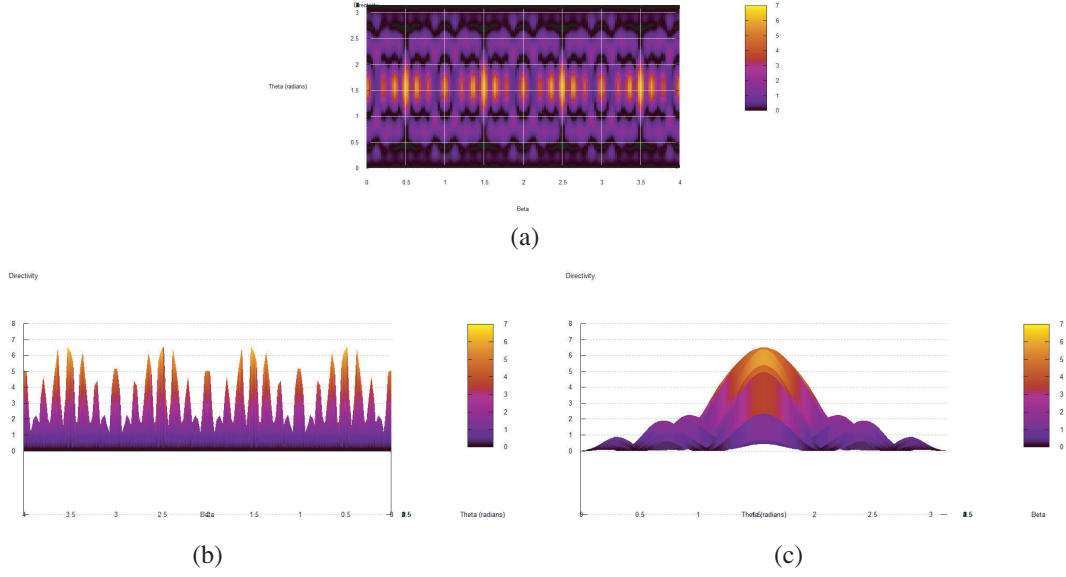


Figure A10. (a) PBM #3 projected onto β - θ plane. (b) PBM #3 projected onto β - D plane. (c) PBM #3 projected onto θ - D plane.

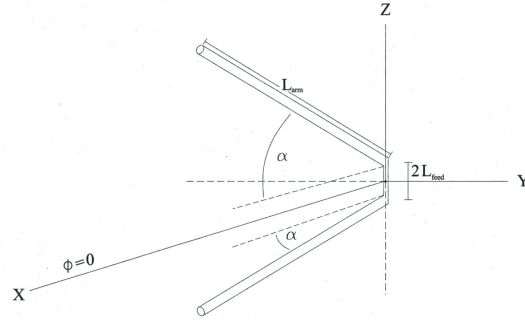


Figure A11. PBM #4 Vee dipole.

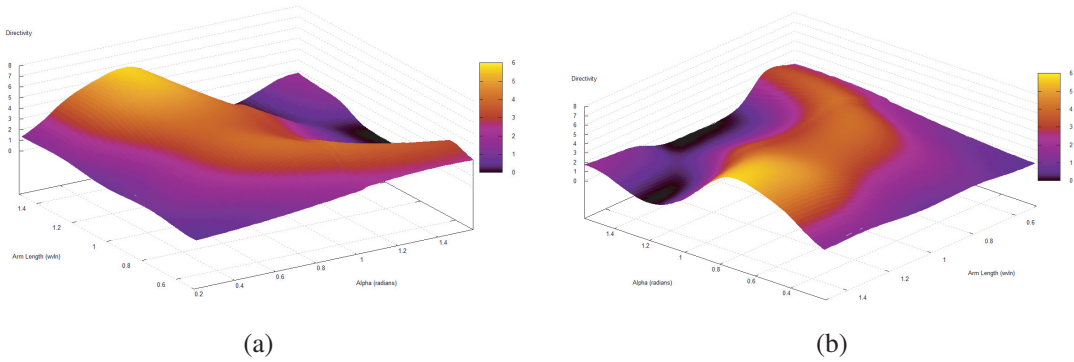


Figure A12. (a) Vee dipole landscape, perspective view. (b) PBM #4 perspective view.

here is $(N_{el} - 1)D$ due to $N_{el} - 1$ spacings in the array. Maximum $D(d_i, i = 1, \dots, N_{el} - 1)$ is independent of N_{el} and occurs at $d_i = 0.99\lambda, \forall i$, that is, all dipoles spaced 0.99λ regardless of the array size. Of course, the value of the directivity itself does depend on the array size, increasing approximately in proportion to the length.

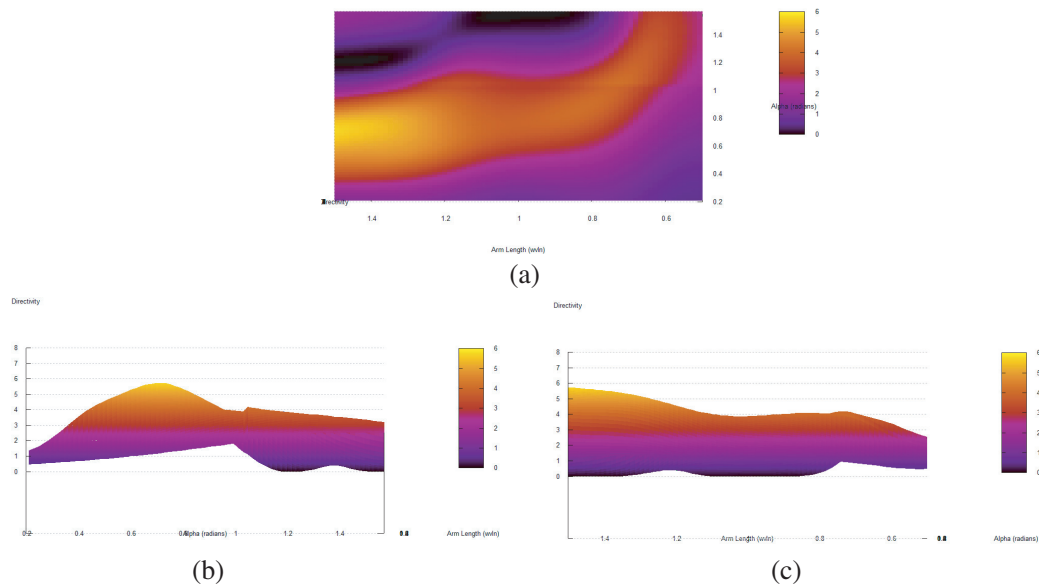


Figure A13. (a) PBM #4 projected onto $L-\alpha$ plane. (b) PBM #4 projected onto $\alpha-D$ plane. (c) PBM #4 projected onto $L-D$ plane.

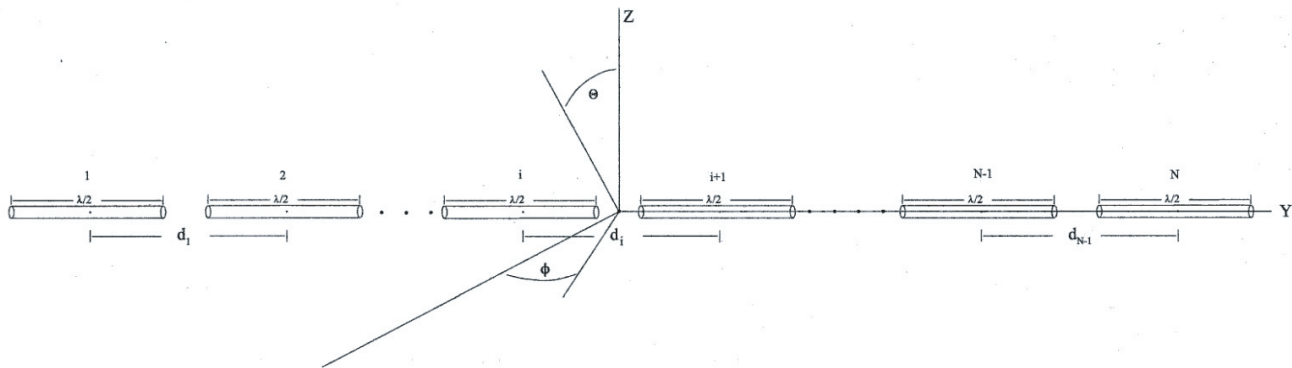


Figure A14. N_{el} -element collinear dipole array.

REFERENCES

1. Dastranj, A., "Optimization of a printed UWB antenna: Application of the invasive weed optimization algorithm in antenna design," *IEEE Antennas & Propagation Magazine*, Vol. 59, No. 1, 48–57, Feb. 2017.
2. Panduro, M. A., C. A. Brizuela, L. I. Balderas, and D. A. Acosta, "A comparison of genetic algorithms, particle swarm optimization and the differential evolution method for the design of scannable circular antenna arrays," *Progress In Electromagnetics Research B*, Vol. 13, 171–186, 2009.
3. Dongho, K., J. Ju, and J. Choi, "A mobile communication base station antenna using a genetic algorithm based Fabry-Pérot resonance optimization," *IEEE Trans. Ant. & Prop.*, Vol. 60, No. 2, 1053, Feb. 2012.
4. Goudos, S. K., "Antenna design using binary differential evolution: Application to discrete-valued design problems," *IEEE Antennas & Propagation Magazine*, Vol. 59, No. 1, 74–93, Feb. 2017.

5. Ni, T., Y.-C. Jiao, L. Zhang, and Z.-B. Weng, "Worst-case tolerance synthesis for low-sidelobe sparse linear arrays using a novel self-adaptive hybrid differential evolution algorithm," *Progress In Electromagnetics Research B*, Vol. 66, 91–105, 2016.
6. Lanza Diego, M., J. R. Perez Lopez, and J. Basterrechea, "Synthesis of planar arrays using a modified particle swarm optimization algorithm by introducing a selection operator and elitism," *Progress In Electromagnetics Research*, Vol. 93, 145–160, 2009.
7. Deb, A., J. S. Roy, and B. Gupta, "Performance comparison of differential evolution, particle swarm optimization and genetic algorithm in the design of circularly polarized microstrip antennas," *IEEE Trans. Ant. & Prop.*, Vol. 62, No. 8, 3920–3928, Aug. 2014.
8. Hosseini, S. A. and Z. Atlasbaf, "Optimization of side lobe level and fixing quasi-nulls in both of the sum and difference patterns by using continuous ant colony optimization (ACO) method," *Progress In Electromagnetics Research*, Vol. 79, 321–337, 2008.
9. Chang, L., C. Liao, W. Lin, L.-L. Chen, and X. Zheng, "A hybrid method based on differential evolution and continuous ant colony optimization and its application on wideband antenna design," *Progress In Electromagnetics Research*, Vol. 122, 105–118, 2012.
10. Cui, C.-Y., Y.-C. Jiao, and L. Zhang, "Synthesis of some low sidelobe linear arrays using hybrid differential evolution algorithm integrated with convex programming," *IEEE Ant. & Wireless Prop. Letters*, Vol. 16, 2017.
11. Rocca, P., G. Oliveri, and A. Massa, "Differential evolution as applied to electromagnetics," *IEEE Antennas & Propagation Magazine*, Vol. 53, No. 1, 38–49, Feb. 2011.
12. Hoorfar, A., "Evolutionary programming in electromagnetic optimization: A review," *IEEE Trans. Ant. & Prop.*, Vol. 55, No. 3, 523–537, Mar. 2007.
13. Coleman, C. M., E. J. Rothwell, and J. E. Ross, "Investigation of simulated annealing, ant-colony optimization, and genetic algorithms for self-structuring antenna," *IEEE Trans. Ant. & Prop.*, Vol. 52, No. 4, 1007–1014, Apr. 2004.
14. Weile, D. S. and E. Michielssen, "Genetic algorithm optimization applied to electromagnetics: A review," *IEEE Trans. Ant. & Prop.*, Vol. 45, No. 3, 343–353, Mar. 1997.
15. Yerrola, A. K. and P. Spandana, "Optimization of linear antennas — A survey," *Int'l. J. Comp. App.*, Vol. 171, No. 3, 17–20, Aug. 2017.
16. Shan, A. and G. G. Wang, "Survey of modeling and optimization strategies to solve high-dimensional design problems with computationally-expensive black-box functions," *Struc. & Multidisc. Opt.*, Vol. 41, 219–241, 2010.
17. Kuwahara, Y., "Multiobjective optimization design of Yagi-Uda antenna," *IEEE Trans. Ant. & Prop.*, Vol. 53, No. 6, 1984–1992, Jun. 2005.
18. Casula, G. A., G. Mazzarella, and N. Sirena, "Evolutionary design of wide-band parasitic dipole arrays," *IEEE Trans. Ant. & Prop.*, Vol. 59, No. 11, 4094–4102, Nov. 2011.
19. Saraereh, O. A., A. A. Saraira, Q. H. Alsafasfeh, and A. Arfoa, "Bio-inspired algorithms applied on microstrip patch antennas: A review," *Int. J. Comm. Ant. & Prop. (I.Re.C.A.P.)*, Vol. 6, No. 6, 336–347, 2016.
20. Pantoja, M. F., A. R. Bretones, and R. G. Martin, "Benchmark antenna problems for evolutionary optimization algorithms," *IEEE Trans. Ant. & Prop.*, Vol. 55, No. 4, 1111–1121, Apr. 2007.
21. Storn, R. and K. Price, "Differential evolution: A simple and efficient adaptive scheme for global optimization over continuous spaces," TR-95-012, ICSI, USA, 1995.
22. Das, A., S. Mullick, and P. N. Suganthan, "Recent advances in differential evolution — An updated survey," *Swarm & Evol. Comp.*, Vol. 27, 1–30, 2016.
23. Zhou, X., G. Zhang, X. Hao, and L. Yu, "A novel differential evolution algorithm using local abstract convex underestimate strategy for global optimization," *Comp. & Op. Res.*, Vol. 75, 132–149, 2016.
24. Tanabe, R. and A. Fukunaga, "Success-history based parameter adaptation for differential evolution," *Proc. IEEE Cong. Evol. Comp. 2013*, 71–78, Cancun, Mexico, 2013.

25. Tanabe, R. and A. Fukunaga, "Improving the search performance of SHADE using linear population size reduction," *Proc. IEEE Cong. Evol. Comp. 2014*, 1658–1665, Beijing, 2014.
26. Liang, J., B. Qu, P. Suganthan, and A. Hernandez-Diaz, "Problem definitions and evaluation criteria for the CEC 2013 special session and competition on real-parameter optimization," Computational Intelligence Laboratory, Zhengzhou University, China and Technical Report, Nanyang Technological University, Singapore, 2013.
27. Liang, J., B. Qu, and P. Suganthan, "Problem definitions and evaluation criteria for the CEC 2014 special session and competition on single-objective real-parameter numerical optimization," Computational Intelligence Laboratory, Zhengzhou University, China and Technical Report, Nanyang Technological University, Singapore, 2014.
28. Zhang, J. and C. Sanderson, "JADE: Adaptive differential evolution with optional external archive," *IEEE Trans. Evol. Comp.*, Vol. 13, No. 5, 945–958, 2009.
29. Isbell, D. E., "Log periodic dipole arrays," *IRE Trans. Ant. & Prop.*, Vol. 8, No. 3, 260–267, May 1960.
30. Jordan, E. C. and K. G. Balmain, *Electromagnetic Waves and Radiating Systems*, 2nd Edition, Chap. 15, Prentice-Hall, Inc., Englewood Cliffs, New Jersey, 1968.
31. Balanis, C. A., *Antenna Theory: Analysis and Design*, Section 11.4, Wiley, New York, 1997.
32. Yang, J., "On conditions for constant radiation characteristics for log-periodic array antennas," *IEEE Trans. Ant. & Prop.*, Vol. 58, No. 5, 1521, May 2010.
33. Lehmensiek, R. and D. I. L. de Villiers, "Optimization of log-periodic dipole array antennas for wideband omnidirectional radiation," *IEEE Trans. Ant. & Prop.*, Vol. 63, No. 8, 3714, Aug. 2015.
34. Lehmensiek, R. and D. I. L. de Villiers, "Constant radiation characteristics for log-periodic dipole array antennas," *IEEE Trans. Ant. & Prop.*, Vol. 62, No. 5, 2966, May 2014.
35. Burke, G. J., "Numerical electromagnetics code — NEC-4.2 method of moments, Part I: User's manual," LLNL-SM-490875, Lawrence Livermore National Laboratory (USA), Livermore, CA, Jul. 2011.
36. Chowdhury, A., A. Ghosh, R. Giri, and S. Das, "Optimization of antenna configuration with a fitness-adaptive differential evolution algorithm," *Progress In Electromagnetics Research B*, Vol. 26, 291–319, 2010.